PRAMANA
— journal of
physics

© Indian Academy of Sciences

Vol. 61, No. 5
November 2003
pp. 865–876

PHOBOS at RHIC: Some global observations*

ALAN S CARROLL, for the PHOBOS Collaboration
B B Back[1], M D Baker[2], D S Barton[2], R R Betts[6], M Ballintijn[4], A A Bickley[7], R Bindel[7], A Budzanowski[3], W Busza[4], A Carroll[2], M P Decowski[4], E García[6], N George[2], K Gulbrandsen[4], S Gushue[2], C Halliwell[6], J Hamblen[8], G A Heintzelman[2], C Henderson[4], D J Hofman[6], R S Hollis[6], R Hołyński[3], B Holzman[2], A Iordanova[6], E Johnson[8], J L Kane[4], J Katzy[4,6], N Khan[8], W Kucewicz[6], P Kulinich[4], C M Kuo[5], W T Lin[5], S Manly[8], D McLeod[6], J Michałowski[3], A C Mignerey[7], R Nouicer[6], A Olszewski[3], R Pak[2], I C Park[8], H Pernegger[4], C Reed[4], L P Remsberg[2], M Reuter[6], C Roland[4], G Roland[4], L Rosenberg[4], J Sagerer[6], P Sarin[4], P Sawicki[3], W Skulski[8], S G Steadman[4], P Steinberg[2,b], G S F Stephans[4], M Stodulski[3], A Sukhanov[2], J-L Tang[5,a], R Teng[8], A Trzupek[3], C Vale[4], G J van Nieuwenhuizen[4], R Verdier[4], B Wadsworth[4], F L H Wolfs[8], B Wosiek[3], K Woźniak[3], A H Wuosmaa[1,c] and B Wysłouch[4]
[1]Argonne National Laboratory, Argonne, IL 60439-4843, USA
[2]Brookhaven National Laboratory, Upton, NY 11973-5000, USA
[3]Institute of Nuclear Physics, Kraków, Poland
[4]Massachusetts Institute of Technology, Cambridge, MA 02139-4307, USA
[5]National Central University, Chung-Li, Taiwan
[6]University of Illinois at Chicago, Chicago, IL 60607-7059, USA
[7]University of Maryland, College Park, MD 20742, USA
[8]University of Rochester, Rochester, NY 14627, USA
[a]Current address: National Chung-Cheng University, Chia-Yi, Taiwan
[b]Current address: University of Cape Town, South Africa
[c]Current address: Western Michigan University, Kalamazoo, MI 49008, USA

Abstract. Particle production in Au+Au collisions has been measured in the PHOBOS experiment at RHIC for a range of collision energies for a large span of pseudorapidities, $|\eta| < 5.4$. Three empirical observations have emerged from this data set which require theoretical examination. First, there is clear evidence of limiting fragmentation. Namely, particle production in central $\mathrm{Au}+\mathrm{Au}$ collisions, when expressed as $\mathrm{d}N/\mathrm{d}\eta'$ ($\eta' \equiv \eta - y_{\mathrm{beam}}$), becomes energy independent at high energy for a broad region of η' around $\eta' = 0$. This energy-independent region grows with energy, allowing only a limited region (if any) of longitudinal boost-invariance. Second, there is a striking similarity between particle production in e^+e^- and $\mathrm{Au}+\mathrm{Au}$ collisions (scaled by the number of participating nucleon pairs). Both the total number of produced particles and the longitudinal distribution of produced particles are approximately the same in e^+e^- and in scaled $\mathrm{Au}+\mathrm{Au}$. This observation

*This presentation is based in large part on the PHOBOS summary talk by M Baker at the *16th Int. Conf. on Ultrarelativistic Nucleus–Nucleus Collisions*, Quark Matter 2002, Nantes, France

was not predicted and has not been explained. Finally, particle production has been found to scale approximately with the number of participating nucleon pairs for $\langle N_{\text{part}} \rangle > 65$. This scaling occurs both for the total multiplicity and for high p_{T} particles ($3 < p_{\text{T}} < 4.5$ GeV/c).

Keywords. Heavy ion; multiplicity; comparison; PHOBOS; RHIC.

PACS Nos 25.75.Dw; 25.75.Nq

1. Introduction

The data described in this paper were taken during the Year 2000 and Year 2001 runs of the relativistic heavy ion collider at Brookhaven National Laboratory. The PHOBOS apparatus [1], shown schematically in figure 1, was used to take data at three energies: $\sqrt{s_{NN}} = 19.6$, 130, and 200 GeV. A partial test detector was also used to take data at $\sqrt{s_{NN}} = 56$ GeV [2].

Unique features of the PHOBOS experiment relevant for the charged particle multiplicity measurements are the large acceptance of the detector and the 12 m long, 1 mm thick, beryllium beam pipe which limits the absorption of low momentum particles and the production of secondaries. The full PHOBOS apparatus comprises two classes of subdetectors. Silicon detectors are employed for vertex finding, particle tracking and multiplicity measurements. This set of detectors has nearly full azimuthal coverage over a large pseudorapidity range $|\eta| < 5.4$. The detector set-up also includes two, fan-shaped arrays of 16 plastic scintillator counters ('paddle counters') located at ± 3.21 m relative to the nominal interaction point along the beam (z) axis. These counters cover pseudorapidity in the range $3 < |\eta| < 4.5$ and served as the primary event trigger. The collision centrality is charac-

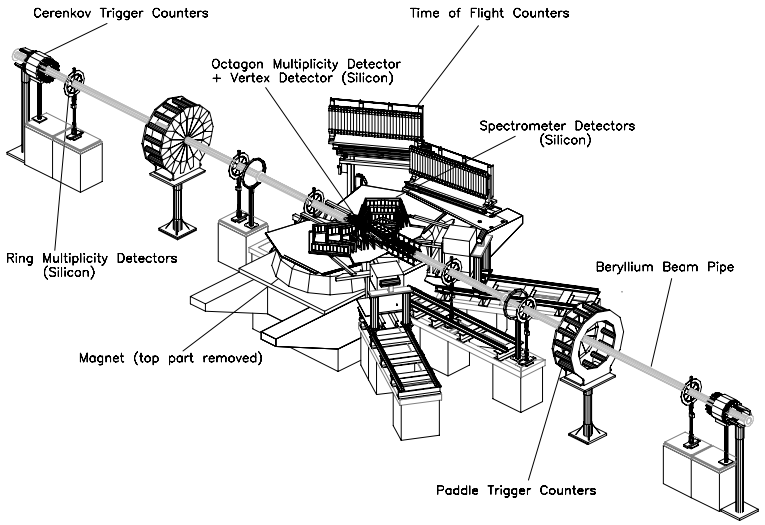

Figure 1. Schematic diagram of the detector set-up for the 2001 running period.

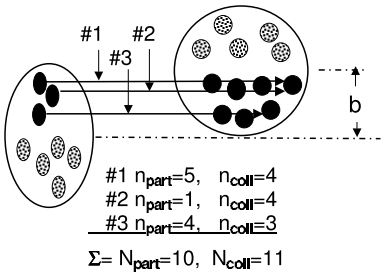

Figure 2. Illustration of the centrality measures used in heavy ion collisions. The filled circles represent the nucleons participating in the interaction. Their size is proportional to the total inelastic cross-section at this $\sqrt{s_{NN}}$. The contributions of three representative nucleons to the $N_{\rm part}$ and $N_{\rm coll}$ measures are shown. The $n_{\rm part}$ of nucleon #2 is only increased by 1 because the four nucleons struck had already been struck by nucleon #1. However, the $n_{\rm coll}$ of #2 is increased by 4 since there are four additional collisions.

terized by the average number of nucleon participants $\langle N_{\rm part}\rangle$, determined as described in refs [3,4].

2. Centrality and multiplicity measurements

The collision centrality is characterized by the average number of nucleon participants $\langle N_{\rm part}\rangle$, determined as described in [3,4]. These references also tabulate the values and systematic errors of $\langle N_{\rm part}\rangle$ for each centrality bin. $\langle N_{\rm part}\rangle$ is equal to the number of 'wounded nucleons'. Another measure often used in heavy ion collisions is $\langle N_{\rm coll}\rangle$ corresponding to the number of 'binary collisions'. Figure 2 illustrates these two measures.

Experimentally, the centrality is determined by matching the monotonically increasing sum of pulse heights in the two paddle counters to a Monte Carlo calculation which utilizes HIJING for the event generator and GEANT for the detector acceptance. $\langle N_{\rm part}\rangle$ is adequately determined from the value of the top 6% down to $\sim$65 participants.

At mid-pseudorapidity ($\eta \simeq 0$) where the particle density is highest in the detectors, four methods are used to cross-check the multiplicity measurements. Two methods involve the formation of two-point straight tracks as shown in figure 3. Because of their simplicity, 'tracklets', require the minimum in the way of corrections due to track reconstruction inefficiencies. The tracklet multiplicity is measured both in the first two planes of the spectrometer and in the vertex planes above and below the beam line.

An octagon-shaped barrel surrounded the interaction region and covered the range $|\eta| < 3.2$. Two sets of 3 ring counters extended the range to $|\eta| < 5.4$. In these single layer detectors, one method for measuring multiplicity was by counting the number of pixels hit and then correcting for occupancy. The second method measured the energy deposited in silicon, and then determined the number of particles from known energy losses.

At mid-rapidity all four of these methods were cross-checked against each other, and away from mid-rapidity, the multiplicity was determined by the latter two methods in the octagon and ring counter detectors.

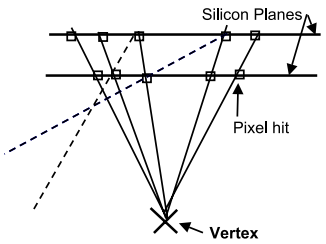

Figure 3. Schematic diagram of 'tracklets' formed by either the spectrometer or vertex silicon planes. All of the possible tracklets formed by pairs of hit pixels must meet at a common vertex (solid lines). Other combinations shown as dotted lines are not included in the count.

3. Survey of basic measurements

A key goal in the design of the PHOBOS experiment was to perform a broad and systematic survey of hadronic particle production in heavy ion collisions. While this survey is still incomplete in terms of energies and species explored, significant progress has been made towards this goal. This section summarizes the basic measurements available so far: multiplicity, particle spectra and azimuthal asymmetry of particle production.

The pseudorapidity densities ($\mathrm{d}N_{\mathrm{ch}}/\mathrm{d}\eta$) and particle yields ($\mathrm{d}^2N/\mathrm{d}y\mathrm{d}p_{\mathrm{T}}$) given here refer to primary produced particles and do not include feed-down products from weak decays of neutral strange particles. Corrections were made for residual effects from secondary interactions and weak decay feed-down as well as for particles which were absorbed or produced in the material surrounding the collision (primarily the beryllium beam pipe and the magnet steel).

Figure 4 shows the charged particle pseudorapidity distributions ($\mathrm{d}N_{\mathrm{ch}}/\mathrm{d}\eta$) measured at $\sqrt{s_{NN}} = 19.6$, 130, and 200 GeV for a variety of centrality bins for pseudorapidity in the range $-5.4 < \eta < 5.4$ [4]. Due to the large coverage in η, $\mathrm{d}N_{\mathrm{ch}}/\mathrm{d}\eta$ is measured over almost the full range, except for a small missing fraction at very high $|\eta|$. For central events, this missing fraction is estimated to be less than 2%. The multiplicity results are discussed further in §§4 and 5.

Figure 5 shows the unidentified charged particle yield measured by PHOBOS for a range of centralities, with rapidity, y_π, defined using the pion mass. These data cover rapidity in the range $0.2 < y_\pi < 1.4$ and transverse momenta in the range $0.2 < p_{\mathrm{T}} < 4.5$ GeV/c, corresponding to six decades of change in the magnitude of the yield.

The unique features of PHOBOS relevant for the momentum-measured particles are the close proximity of the detector to the interaction region (10–80 cm), the precise vertex determination (0.1–0.3 mm), good segmentation (0.4–1 mm) of the silicon detectors in the bend direction and, again, the small amount of material between the interaction and the first layers of silicon. As indicated in figure 5, these features allow the measurement of particles with good momentum resolution over a broad range of transverse momenta from 0.03 to 5.0 GeV/c [7], and beyond (when statistics allow), as well as providing the ability to reject most secondaries and decay products.

The broad p_{T} range, particularly the coverage to very low p_{T}, will be important for constraining the role of dynamical processes such as rescattering and radial expansion in these collisions. The charged particle multiplicity (and elliptic flow) measurement spans

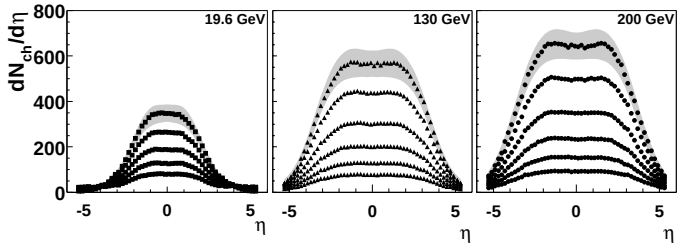

Figure 4. Charged particle pseudorapidity distribution, $\mathrm{d}N_{\mathrm{ch}}/\mathrm{d}\eta$, measured for Au + Au at $\sqrt{s_{NN}} = 19.6$, 130, and 200 GeV for the centrality bins: 0–6% (the most central collisions), 6–15%, 15–25%, 25–35%, 35–45%, 45–55%. The most peripheral bin is excluded for the lowest energy. The statistical error is negligible. The typical systematic error is shown as a 90% C.L. band for selected centrality bins.

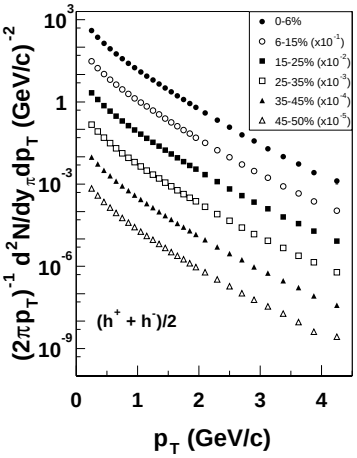

Figure 5. Charged particle invariant yields in Au + Au collisions for six centrality bins. For clarity, consecutive bins are scaled by factors of 10. Statistical and systematic uncertainties are smaller than the symbol size.

roughly 11 units of pseudorapidity, 2π in azimuth, and a factor of 10 in beam energy, in a single experiment, providing strong constraints on any description of the initial state and subsequent dynamics [5–7]. From this broad data set, three empirical scaling rules have emerged. Sections 4–6 describe each of them in turn. These rules, at the very least, provide a compact description of the data which must be respected by any model. At best, these empirical scaling rules may point the way to a more accurate description of the dynamics of these collisions.

4. The limiting curve for particle production

The pseudorapidity distributions were shown in figure 4 for three different collision energies ($\sqrt{s_{NN}}$). In order to separate the trivial kinematic broadening of the $\mathrm{d}N_{\mathrm{ch}}/\mathrm{d}\eta$ dis-

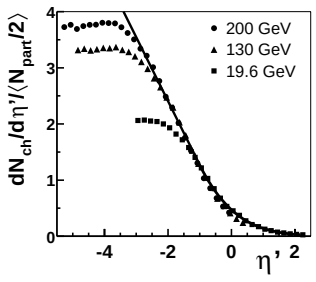

Figure 6. Shifted pseudorapidity distribution, $\mathrm{d}N_{\mathrm{ch}}/\mathrm{d}\eta'$ per participant pair, where $\eta' \equiv \eta - y_{\mathrm{beam}}$, for Au + Au data at $\sqrt{s_{NN}} = 19.6$, 130, and 200 GeV. Systematic errors not shown. The curve is to 'guide the eye'.

tribution from the more interesting dynamics, the data for Au + Au collisions at different energies can be viewed in the rest frame of one of the colliding nuclei. Such an approach led to the ansatz of 'limiting fragmentation' [8], which successfully predicted the energy dependence of particle production away from mid-rapidity in hadron collisions, including pA [9] and $p\bar{p}$ [10]. This ansatz states that, at high enough collision energy, both $\mathrm{d}^2N/\mathrm{d}y'\mathrm{d}p_{\mathrm{T}}$ and the mix of particle species (and therefore also $\mathrm{d}N/\mathrm{d}\eta'$) reach a limiting value and become independent of energy in a region around $y' \sim 0$, where $y' \equiv y - y_{\mathrm{beam}}$ and rapidity $y \equiv \tanh^{-1}\beta_z$, with the $\hat{z}$-axis defined as the beam (collision) axis.

Figure 6 shows the scaled, shifted pseudorapidity distributions $\mathrm{d}N_{\mathrm{ch}}/\mathrm{d}\eta'/\langle N_{\mathrm{part}}/2\rangle$ [4]. The results are folded about mid-rapidity (positive and negative η bins are averaged). The distributions are observed to be independent of collision energy over a substantial η' range. This is consistent with and extends a similar observation made by BRAHMS [11] over a more restricted η' range. Both the 19.6 and 130 GeV data reach 85–90% of their maximum value before deviating significantly (more than 5%) from the common limiting curve.

The data presented here demonstrate that limiting fragmentation applies in the Au + Au system, and that the 'fragmentation region' in Au + Au is rather broad, covering more than half of the available range of η' over which particles are produced. In particular, the fragmentation region grows significantly between 19.6 GeV and 130 GeV, extending more than two units away from the beam rapidity. Particle production appears to approach a fixed limiting curve which extends far from the original beam rapidity, indicating that this limiting curve is an important feature of the overall interaction and not simply a nuclear breakup effect. This result is in sharp contrast to the boost-invariance scenario [12] which predicts a fixed fragmentation region and a broad central rapidity plateau that grows in extent with increasing energy.

5. Similarity of AA and e^+e^- at high energy

In the upper part of figure 7, total charged multiplicity data from pp, $p\bar{p}$, e^+e^-, and AA (scaled by $\langle N_{\mathrm{part}}\rangle/2$) are shown as a function of the appropriate $\sqrt{s}$ for each system. See [13] for more details and [14] for the non-PHOBOS data. The e^+e^- data serves as a reference sample, describing the behavior of a simple color dipole system with a large $\sqrt{s}$. The curve is a description of the e^+e^- data, given by the functional form: $C\alpha_{\mathrm{s}}(s)^A \mathrm{e}^{\sqrt{B/\alpha_{\mathrm{s}}(s)}}$

with the parameters A and B calculable in perturbative QCD and the constant parameter C determined by a fit to the e^+e^- data [15]. In order to compare them with e^+e^-, the pp and $p\bar{p}$ data were plotted at an effective energy $\sqrt{s_{\rm eff}} = \sqrt{s}/2$, which approximately accounts for the 'leading particle effect' [16]. Finally, central AA collisions, Au + Au from the AGS and RHIC, and Pb + Pb from CERN are shown. Over the available range of RHIC energies from 19.6 to 200 GeV, the Au + Au results are consistent with the e^+e^- results, suggesting a universality of particle production at high energy.

In addition, the Au + Au data approximately agrees with the scaled pp and $p\bar{p}$ data suggesting that the effective energy of a high energy AA collision is approximately just $\sqrt{s_{NN}}$. The lower part of figure 7 shows the same results, but divided by the e^+e^- fit. This figure illustrates the approach of AA from lower energies towards the high energy scaling result.

Figure 8 compares the pseudorapidity distribution for central Au + Au collisions to the closest available analog in e^+e^- collisions: the thrust-axis-rapidity distribution, where the pion mass was used for all charged particles in e^+e^- [17]. This shows that particle production in Au + Au and e^+e^- collisions approximately agree in longitudinal particle distribution as well as in the total yield.

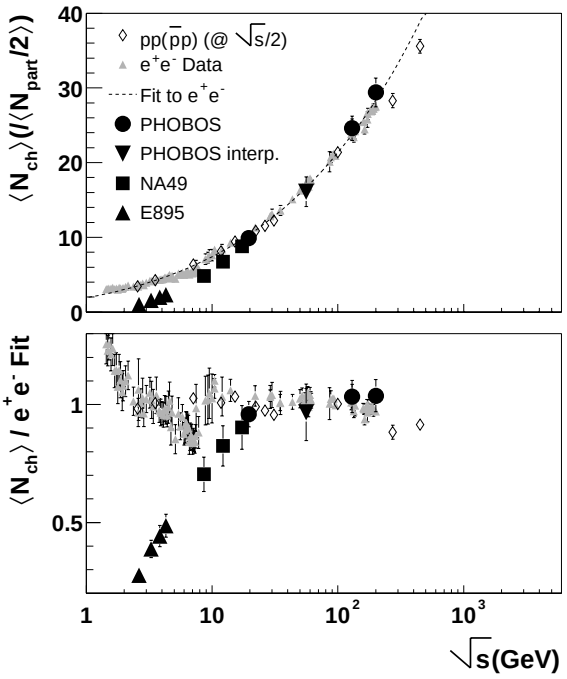

Figure 7. Comparison of the total charged multiplicity vs. collision energies for AA, e^+e^-, pp, and $p\bar{p}$ data, as described in the text. In the upper panel, the curve is a perturbative QCD expression fit to the e^+e^- data. In the lower panel, the data have all been divided by the e^+e^- fit.

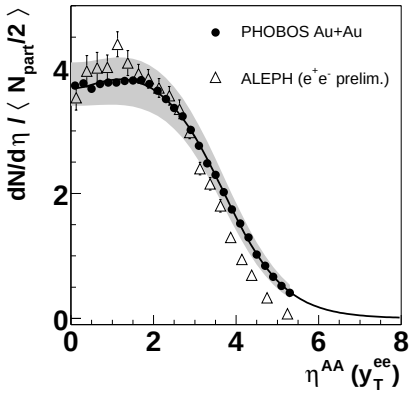

Figure 8. Pseudorapidity distribution of charged particles produced in central Au + Au collisions at $\sqrt{s_{NN}} = 200$ GeV compared with the rapidity distribution along the thrust axis of particles produced in e^+e^- collisions at $\sqrt{s} = 200$ GeV. The Au + Au data are normalized by $N_{\text{part}}/2$. Systematic errors are shown for the Au + Au data.

6. Participant scaling of particle production

Participant scaling was first established in the context of the total charged particle multiplicity produced in pA collisions [18]. In high energy AA collisions, small deviations from participant scaling for mid-rapidity $\mathrm{d}N/\mathrm{d}\eta$ have been seen. For instance, figure 9 shows the mid-rapidity $\mathrm{d}N/\mathrm{d}\eta$ scaled by $\langle N_{\text{part}}\rangle/2$ measured with the same apparatus for $\sqrt{s_{NN}} = 19.6$, 130, and 200 GeV. Results of this type are sometimes interpreted in terms of a mixture of 'hard' and 'soft' components scaling as $N_{\text{part}}^{4/3}$ and N_{part} respectively [19]. This interpretation is somewhat ambiguous, however, since saturation models [19,20] describe the data more economically, as can be seen in figure 9, and since both dynamic and kinematic effects can shift particles around in pseudorapidity as centrality changes.

Due to the large acceptance of the PHOBOS detector, we can integrate the total charged particle production in these collisions. Figure 10 shows $N_{\text{ch}}/\langle N_{\text{part}}/2\rangle$ as a function of $\langle N_{\text{part}}\rangle$ for the three different energies. Also shown are the equivalent results for pp and $p\bar{p}$ as well as e^+e^- collisions at the same values of $\sqrt{s}$. It should be noted that the $pp/p\bar{p}$ data are shown at their collision $\sqrt{s}$ for this plot and not $\sqrt{s_{\text{eff}}}$. Three conclusions can be drawn from this result. First, total charged multiplicity in high energy AA collisions approximately scales with wounded nucleons (N_{part}). Second, total particle production in AA collisions per participant pair is the same as the total particle production in e^+e^- at the same energy for a broad range of centralities, not just for central collisions. Finally, particle production in pp and $p\bar{p}$ collisions is reduced compared to AA and e^+e^-.

While the overall charged particle production scales with N_{part}, at high p_{T}, particle production is expected to scale with $N_{\text{coll}} \propto N_{\text{part}}^{4/3}$. Deviations from this scaling at high p_{T} are likely to indicate high density effects in the initial or final state. PHENIX and STAR have already shown that high p_{T} hadron production is suppressed with respect to

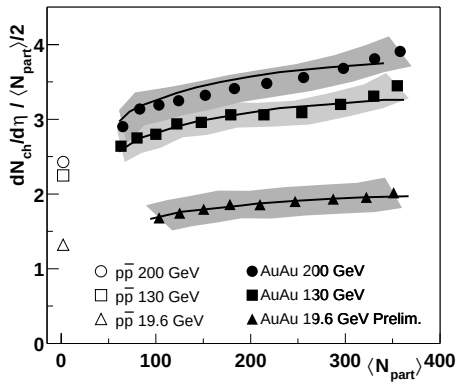

Figure 9. Scaled pseudorapidity density at mid-rapidity, $\mathrm{d}N/\mathrm{d}\eta/\langle N_{\mathrm{part}}/2\rangle$, as a function of centrality for 19.6, 130, and 200 GeV. The curves correspond to predictions from the saturation model [19,20].

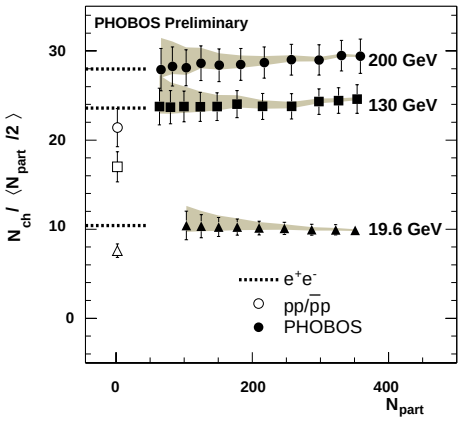

Figure 10. Total charged multiplicity normalized by $\langle N_{\mathrm{part}}/2\rangle$ as a function of N_{part} for AA. Also shown are results for e^+e^- and $p\bar{p}$ data.

$N_{\mathrm{coll}} \times \sigma_{pp\to hX}$ [21]. Recalling that figure 10 indicates that pp collisions may not be the ideal reference sample, we investigate the scaling of high p_{T} hadron production in AA collisions internally, using a mid-central Au + Au collision as a reference rather than pp data.

In figure 11, $\mathrm{d}^2N/\mathrm{d}y\mathrm{d}p_{\mathrm{T}}/\langle N_{\mathrm{part}}/2\rangle$ is shown as a function of $\langle N_{\mathrm{part}}\rangle$ as normalized to the yield $\langle N_{\mathrm{part}}/2\rangle$ in the most peripheral bin [22]. The centrality bins used here are specified in figure 5. The expectation for $\langle N_{\mathrm{coll}}\rangle$-scaling relative to the most peripheral bin is shown as a dashed line. The solid curves give the expectation for $\langle N_{\mathrm{part}}\rangle$-scaling relative to the most peripheral bin. $\langle N_{\mathrm{coll}}\rangle$ increases from 107 to 1050 over the centrality range. No corresponding increase in particle production per participant at $p_{\mathrm{T}} = 3$ GeV/c and above is observed. The yields in this region scale approximately with $\langle N_{\mathrm{part}}\rangle$. This confirms the empirical observation that particle production at high p_{T} is suppressed with respect to the 'hard scaling' expectation. However, we note the additional intriguing fact that, for $N_{\mathrm{part}} > 65$, we see approximate N_{part} scaling of both low and high p_{T} particle production. Mid-range particles with $p_{\mathrm{T}} \sim 1.5$ GeV/c show a small violation of N_{part} scaling, but are still suppressed with respect to the naive scaling expectations. This particular form of 'high p_{T} suppression' could be an indication of initial state suppression (e.g. parton saturation) or that the final state suppression (e.g. 'jet quenching') reaches a geometric maximum involving one power of length scale $R_{\mathrm{Au}} \propto N_{\mathrm{part}}^{1/3}$. Of course, this apparent N_{part} scaling could also be accidental.

7. Summary

The PHOBOS experiment has measured a systematic data set of Au+Au collisions at the RHIC collider. These data span an energy range from $\sqrt{s_{NN}} = 19.6$ to 200 GeV, a

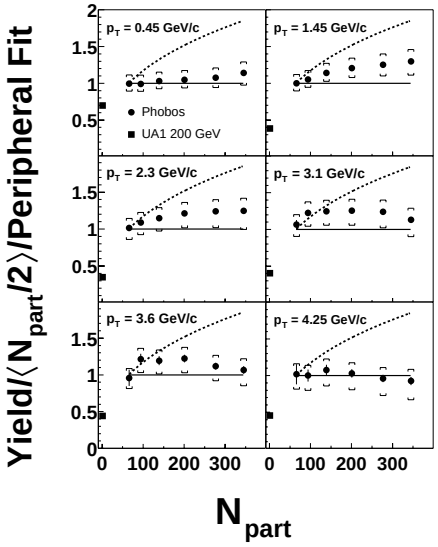

Figure 11. Charged hadron yields per participant pair in six different transverse momentum bins, plotted as a function of $\langle N_{\rm part}\rangle$. The data are normalized to the yield in the most peripheral centrality bin. The dashed (solid) line shows the expectation for the $\langle N_{\rm coll}\rangle$ ($\langle N_{\rm part}\rangle$) scaling from peripheral to central collisions. The brackets indicate the systematic uncertainty for the centrality evolution of this ratio (90% C.L.).

pseudorapidity range from -5.4 to $+5.4$ and a centrality range from 65 to 340 participating nucleons. It also includes particle spectra covering the $p_{\rm T}$ range from 0.03 to 5.0 GeV/c.

Three empirical observations have emerged from this data set. First, there is clear evidence of limiting fragmentation in Au + Au collisions: an energy-independent region of η' ($\eta' \equiv \eta - y_{\rm beam}$). This energy-independent region grows with energy, allowing only a limited region (if any) of longitudinal boost-invariance. Second, there is a striking, unexpected, similarity of particle production in e^+e^- and particle production per participating nucleon pair in Au + Au collisions. Finally, particle production has been found to approximately scale with the number of participating nucleon pairs for $\langle N_{\rm part}\rangle > 65$. This scaling occurs for the total multiplicity and also for high $p_{\rm T}$ particles (including $3 < p_{\rm T} < 4.5$ GeV/c).

These empirical observations serve, at least, to characterize heavy ion collisions in an economical way and to challenge models. At best, the observed scaling and universalities may point the way to a fairly simple partonic description of this high density matter and thus advance our knowledge of the strong interaction.

8. Addendum

In the absence of representatives from the other RHIC experiments, brief summaries of results from the PHENIX and STAR Collaborations related to evidence at large $p_{\rm T}$ of possible QGP formation were presented. These were the evidence of jet quenching from

PHENIX [23], and the observation of the suppression of away side jets by the STAR Collaboration [24].

Acknowledgements

This work was partially supported by US DOE grants DE-AC02-98CH10886, DE-FG02-93ER40802, DE-FC02-94ER40818, DE-FG02-94ER40865, DE-FG02-99ER41099, and W-31-109-ENG-38 as well as NSF grants 9603486, 9722606 and 0072204. The Polish group was partially supported by KBN grant 2-P03B-10323. The NCU group was partially supported by NSC of Taiwan under contract NSC 89-2112-M-008-024.

References

[1] B B Back *et al*, *Nucl. Instrum. Methods*, to be published
R Nouicer *et al*, *Nucl. Instrum. Methods* **A461**, 143 (2001)
B B Back *et al*, *Nucl. Phys.* **A698**, 416c (2002)
[2] B B Back *et al*, *Phys. Rev. Lett.* **85**, 3100 (2000)
[3] B B Back *et al*, *Phys. Rev.* **C65**, 061901R (2002)
[4] B B Back *et al*, arXiv:nucl-ex/0210015; *Phys. Rev. Lett.* (submitted)
[5] B B Back *et al*, arXiv:nucl-ex/0205021; *Phys. Rev. Lett.* (in press)
[6] S Manly *et al*, *Proceedings of 16th International Conference on Ultrarelativistic Nucleus–Nucleus Collisions* (Quark Matter 2002 (QM 2002), Nantes, France); arXiv:nucl-ex/0210036
[7] B Wosiek *et al*, *Proceedings of 16th International Conference on Ultrarelativistic Nucleus–Nucleus Collisions* (Quark Matter 2002 (QM 2002), Nantes, France); arXiv:nucl-ex/0210037
[8] J Benecke, T T Chou, C-N Yang and E Yen, *Phys. Rev.* **188**, 2159 (1969)
[9] J E Elias *et al*, *Phys. Rev.* **D22**, 13 (1980)
[10] G J Alner *et al*, *Z. Phys.* **C33**, 1 (1986)
[11] I G Bearden *et al*, *Phys. Rev. Lett.* **88**, 202301 (2002)
[12] J D Bjorken, *Phys. Rev.* **D27**, 140 (1983)
[13] P A Steinberg *et al*, *Proceedings of 16th International Conference on Ultrarelativistic Nucleus–Nucleus Collisions* (Quark Matter 2002 (QM 2002), Nantes, France); arXiv:nucl-ex/0211002
B B Back *et al*, *Phys. Rev. Lett.* (submitted); arXiv:nucl-ex/0301017
[14] J Klay and U C Davis, Ph.D. Thesis (2001)
S V Afanasiev *et al*, arXiv:nucl-ex/0205002 (2002)
D E Groom *et al*, *Euro. Phys. J.* **C15**, 1 (2000)
[15] A H Mueller, *Nucl. Phys.* **B213**, 85 (1983)
[16] M Basile *et al*, *Phys. Lett.* **B92**, 367 (1980)
M Basile *et al*, *Phys. Lett.* **B95**, 311 (1980)
[17] P Abreu *et al*, *Phys. Lett.* **B459**, 397 (1999)
[18] J E Elias *et al*, *Phys. Rev. Lett.* **41**, 285 (1978)
A Białas, B Bleszyński and W Czyż, *Nucl. Phys.* **B111**, 461 (1976)
[19] D Kharzeev and M Nardi, *Phys. Lett.* **B507**, 121 (2001)
[20] D Kharzeev and E Levin, *Phys. Lett.* **B523**, 79 (2001)
D Kharzeev, E Levin and M Nardi; arXiv:hep-ph/0111315
[21] K Adcox *et al*, *Phys. Rev. Lett.* **88**, 022301 (2002)
C Adler *et al*, *Phys. Rev. Lett.* **89**, 202301 (2002)

[22] C Roland *et al*, *Proceedings of 16th International Conference on Ultrarelativistic Nucleus–Nucleus Collisions* (Quark Matter 2002 (QM 2002), Nantes, France)
[23] K Adcox *et al*, arXiv:nucl-ex/0207009 (2002); *Phys. Lett. B* (submitted)
[24] C Adler *et al*, *Phys. Rev. Lett.* **90**, 082302 (2003)